Pergamon

Int. J. Heat Mass Transfer. Vol. 38, No. 2, pp. 207–217, 1995

0017-9310/95 $9.50+0.00

0017-9310(94)00165-0

Aerothermic characterization of a high-power fast axial flow CO_2 laser

O. BOIRON, G. LE PALEC and PH. BOURNOT

Institut Méditerranéen de Technologie, Unité Lasers de Puissance, Technopôle de Château-Gombert, 13451 Marseille Cedex 20, France

(*Received* 26 *March* 1993 *and in final form* 6 *June* 1994)

Abstract—Because the structure of the flow in glow discharge tubes for high-power CO_2 lasers is one of the main physical processes to control in order to avoid arcing, an experimental procedure for studying the velocity and temperature fields in such tubes was performed. Two kinds of injection system have been studied. For the first one, the gas mixture is injected by a single sonic nozzle located on the axis of the tube. Because the power of the laser may be increased by associating several tubes in line, the other injection system consists of a series of 12 holes radially arranged in order to move injectors away from the axis. For both cases, the axial mean time velocity profile was measured (without electric discharge) using a laser Doppler anemometry technique in several sections of the discharge tube. The temperature field was investigated during the discharge by using a special thermofluorescent probe. It is found that turbulence facilitates the homogenization of the discharge.

1. INTRODUCTION

Nowadays, the electrical discharge CO_2 laser is more and more used in laboratories and industrial processes (welding, cutting,...) as a high-performance tool. The power range actually available is about a few watts for wave-guide CO_2 lasers, 10^4 W for fast transversal flow lasers and 10^8 W for preionized TEA lasers operating in the pulsed mode. Although the physical processes occurring in all these lasers are similar, their performances are different because of the technological choices retained for their conception. Among the parameters having a significant effect upon the discharge, the geometry of the laser cavity, the pressure and velocity fields, the temperature of the gas mixture and the electronic density are of the greatest interest.

For fast axial flow lasers, the axis of the gas flow and optical axis merge with the axis of the electrical discharge. The linear energy laser extracted from the tube is about 300 W m^{-1} [1, 2], the gas flow structure being similar to a subsonic one for cylindrical geometry tubes. From all these characteristics, it follows that most of the Joule effect energy is delivered in the region of the axis tube, which can induce arcing under high-pressure operating conditions.

A 10 kW turbulent axial flow CO_2 laser (TAF 10) has been developed at the 'Institut Méditerranéen de Technologie' in Marseille: this laser is a fast axial flow laser equipped with 12 discharge tubes, as shown in Fig. 1 [3]. In order to move injectors away from the optical axis of the laser cavity, 12 sonic nozzles are radially arranged in each tube. The high subsonic turbulent flow which results from the mixing of the 12 jets allows us avoid the arcing phenomenon. The delivered electrical power is about 5 kW for each tube. This paper presents an experimental investigation of the velocity and temperature fields in such a tube. In order to test the validity of results, the case of injection by means of a single sonic nozzle located in the axis of the entrance section of the tube is also investigated: indeed, the flow structure is then axisymmetric and such a configuration has been the subject of a few experimental and theoretical studies [4–7].

2. EXPERIMENTAL PROCEDURE

2.1. *The testing bench*

The principle of the testing bench is shown in Fig. 2: three roots are arranged in parallel with each other and deliver 1000, 2000 and 4000 m^3 h^{-1}, respectively, in the gas circulating closed cycle. The compression ratio is 2.5 for a maximal inlet pressure of 50 mb. At the exit of each root, a gas–water heat exchanger is placed, so that the injection gas temperature is maintained at 17°C. Because the maximal temperature sup-

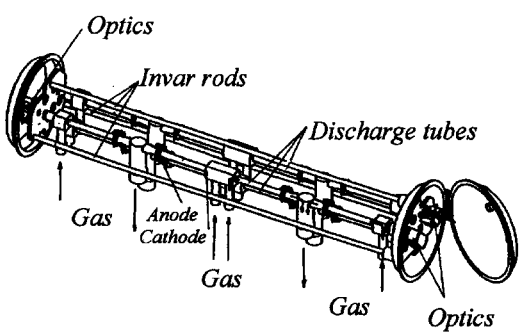

Fig. 1. Schematic diagram of the 10 kW laser head [3].

NOMENCLATURE

a_t	speed of the sound at the throat section [m s^{-1}]	T_{up}	temperature upstream of the nozzle [K]
Cp	specific heat [J kg^{-1} K^{-1}]	T_{down}	temperature in the exit section of the discharge tube [K]
D	inner diameter of the discharge tube [m]	U	local mean velocity of the gas mixture [m s^{-1}]
f	focal length [m]	U_e	mean velocity in the exit section of the discharge tube [m s^{-1}]
h	heat transfer coefficient [W m^{-2} K^{-1}]	U_0	mean time velocity on the axis of the discharge tube [m s^{-1}]
I	intensity [A]	U_{rms}	root mean square instantaneous velocity [m s^{-1}]
k	thermal conductivity [W m^{-1} K^{-1}]	V	voltage [V]
L	length of the discharge tube [m]	X	distance from the throat section [m].
P_{down}	pressure in the exit section of the discharge tube [Pa]		
P_{up}	pressure upstream of the nozzle [Pa]	Greek symbols	
r	radial distance from the axis of the discharge tube [m]	μ	dynamic viscosity [kg m^{-1} s^{-1}]
S	exchange area in boundary conditions (A3)–(A6) [m^2]	ρ	density [kg m^{-3}].
T	temperature [K]		
T_0	temperature on the axis of the discharge tube [K]		

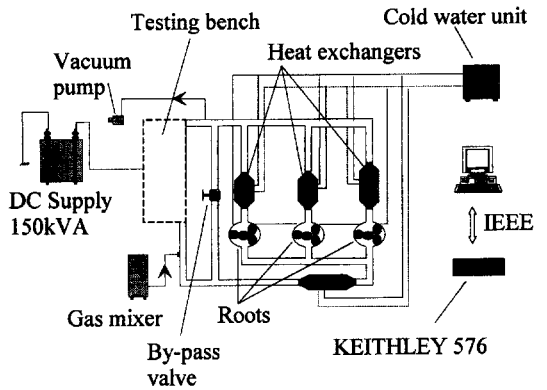

Fig. 2. Gas recirculating loop.

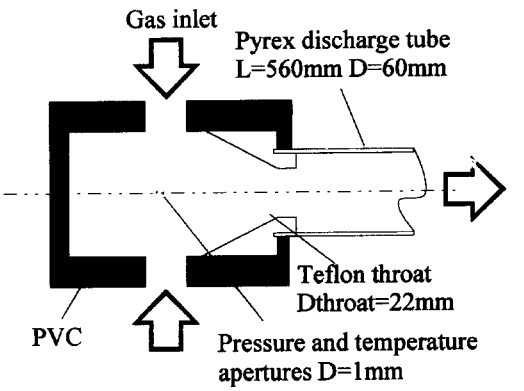

Fig. 3.(a) Axial injector. (b) Radial injector system (as for the TAF 10 laser).

ported by the roots is 120°C, the hot gases coming from the discharge tube must be cooled before compression, so that another heat exchanger is placed between the tube and the roots. The gas flow-rate is regulated with a bypass valve and the maximal value of the mean velocity is about 350 m s^{-1} for a discharge tube with a 60 mm diameter. For air, the corresponding Reynolds number is 60 000 when the static pressure is 50 mb. This low pressure is generated with a vacuum pump, the measured maximum value of the depressurizarion being 0.1 mb h^{-1} during 24 h. A data acquisition and treatment system gives real-time measurements of temperature and pressure fields at several locations in the gas circulating closed cycle, so that the gas flow-rate can be automatically adjusted.

Two systems of injection have been tested on Pyrex tubes with a 60 mm inner diameter and 0.6 m between the two electrodes. These two injectors are made with Teflon:

(i) The first one [Fig. 3(a)] is an injector which consists of a single sonic nozzle located on the axis of

the tube, the tungsten electrode being placed on the axis of the nozzle. The theoretical velocity is 50 m s^{-1} with a pressure of 50 mb in the exit section of the tube, the ratio between entrance pressure and exit pressure being 1.89.

(ii) The other injector [Fig. 3(b)] is an annular-type one which has 12 sonic nozzles radially arranged. The diameter of the throats is 8.5 mm and a tungsten electrode is inserted in each one. All the electrodes are connected in parallel by means of 10 kW 'ballast' resistances. The theoretical average speed is then 92 m s^{-1}, when sonic conditions are realized.

The electrical supply is a 150 KVA DC supply delivering a continuous voltage. The current and voltage delivered are measured with a Hall effect probe and a high-voltage probe, respectively.

2.2. *The laser Doppler anemometry bench*

In order to get some information about the turbulence structure flow in the discharge tube, hot-wire anemometry and laser Doppler anemometry (LDA) techniques may be performed. The latter one was selected because it avoids calibration problems. The velocimetry apparatus is a DANTEC 55L90, with which it is possible to measure particle velocities as high as 515 m s^{-1}. A transmitter optic with a focal length $f = 600$ mm is connected to an ionized argon laser by means of a single mode fiber optic transducer: this can transmit a 1 W beam under the TEM_{00} mode. The transmitter optic is placed so that the two incident beams are coplanar with the axis of the tube. These beams pass through the air–Pyrex (external) and Pyrex–gas (inner) interfaces of the wall tube with a constant difference of 0.6 mm compared to the radial line of sight. The photomultiplier ($f = 300$ mm) operates in the forward scattering position.

Two kinds of aerosols have been tested:

(i) Liquid aerosols generated from a mixing of glycerine and water which was pulverized by means of a TSI 9302 atomizer. The estimated size of such particules is from 5 to 10 μm. Unfortunately, it was impossible to obtain good experimental results with these particles because of the too low aerosol concentration in the gas mixture. Indeed, the main problem is to maintain a constant pessure (70 mb) in the whole gas circulating loop during injection of aerosols,

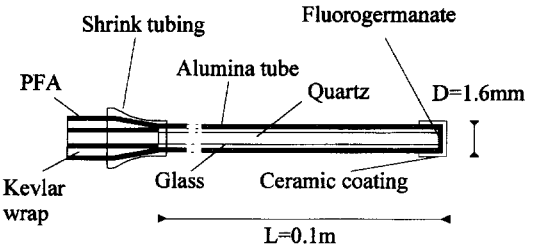

Fig. 5. Fluoroptic probe.

which was impossible with the vacuum pump performances used for these experiments.

(ii) Submicronic smoke particles: this was the only way to get sufficiently high concentration particles with this vacuum pump. The smoke is extracted from a cylindrical tank in which the air flow is pulsed in order to create a process similar to a cyclone generation: the smoke is then injected into the gas circulating closed cycle, the branching zone being located approximately 1 m upstream of the nozzles.

2.3. *The optical fiber temperature control system*

Temperatures have been measured during the electrical discharge by means of a fluorescent thermometer [8, 9], the principle of which being shown in Fig. 4. The main element of this system is the temperature sensor which consists of a small amount of temperature-sensitive phosphorus located at the top of the fiber optic probe (see Fig. 5). When the phosphorus is excited with blue light, it exhibits a deep red fluorescence.

The pulse of optical energy which is needed to excite the phosphorus to fluorescence is provided by a xenon flash lamp. After the pulse is over, the intensity of radiation decays. The fluorescent decay time is measured and then correlated with the phosphorus temperature: this is done by comparison between the value of the decay time and a calibration value stored in the computer memory. The temperature data are transmitted by a RS-232-C port to an external PC-AT micro-computer.

Figure 6 shows a cross-section of the discharge tube with the probe: the latter is introduced into a 2 mm diameter hole located at the top of the tube by means

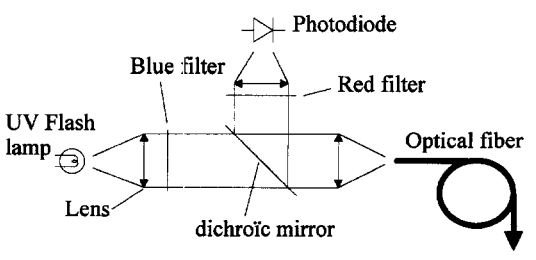

Fig. 4. Fluoroptic thermometer.

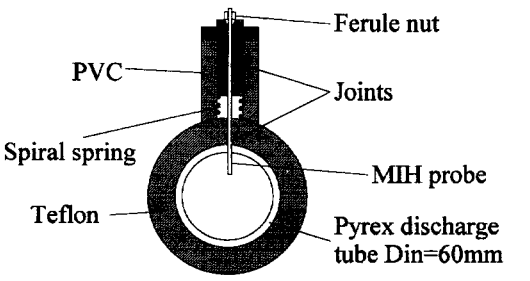

Fig. 6. Temperature measurement system.

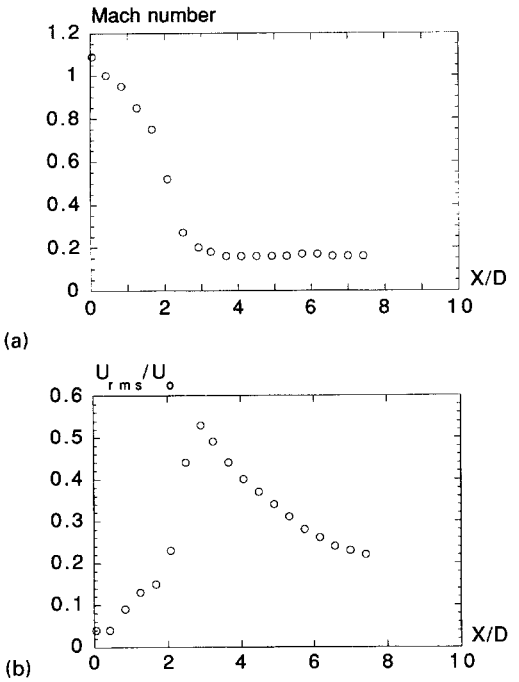

Fig. 7. (a). Variation of the mean time velocity along the axis of the tube (axial injector) $Re = 6700$, $P_{down} = 30$ mb. (b) Turbulence intensity along the axis of the tube (axial injector). $Re = 6700$, $P_{down} = 30$ mb.

of a mechanical system which ensures pressure insulation. Six holes have been made along the discharge tube, allowing us to obtain radial temperature profiles for several sections.

3. RESULTS AND DISCUSSION

3.1. *Velocity field in the discharge tube*

For the two kinds of injectors (i.e. the axial injector and radial injectors), the axial component velocity profiles have been measured with sonic conditions at the throat(s) where the speed of the sound, a_t, is 341 m s^{-1} for air at 17°C. The Reynolds number is defined as $Re = \rho U_e D/\mu$, U_e being the mean velocity at the exit section and D the inner diameter of the discharge tube; ρ and μ, respectively, denote the density and dynamic viscosity of the gas. The physical properties of the gas are calculated for exit conditions. The Mach number is defined as U/a_t. Results are presented in dimensionless form: the reference length is the diameter (D) of the tube for axial profiles and the radius (R) of the tube for radial profiles.

3.1.1. *Axial injector.* For the axial injector case, Fig. 7(a) and (b) respectively, show the mean time axial velocity profile and the turbulence intensity (U_{rms}/U_0, U_0 denoting the local mean time velocity on the axis of the tube) along the axis of the discharge tube. Although the pressure ratio was determined in order to have a subsonic–sonic–subsonic flow configuration, it is seen that, near the throat ($X = 0$), the axial Mach number is greater than unity: the reason is that the stagnation pressure in the injection chamber is higher than the measured static pressure, which is due to the fact that the velocity of the gas in the chamber is not equal to zero as assumed for the calculation of the pressure ratio. The axial velocity highly decreases with an accompanying radial expansion between $X/D = 0$ and $X/D \approx 3$, this last point corresponding to the reattachment zone. The flow then redevelops up to the exit section.

In the separated region, the recirculating flow interacts with the jet and thus creates a high-shear zone which induces a maximal turbulence intensity. This maximum is approximately located at $X/D = 2$. The results which have been obtained agree with those reported by Hégo [7] who used a hot-wire anemometry technique: however, for this geometry, the LDA technique used in the present study allows us to perform measurements nearer the throat region.

3.1.2. *Radial injectors.* Figure 8(a)–(c) corresponds to the radial injectors for which it was technically impossible to measure near the throats region. This is why no experimental points are reported for $0 \leqslant X/D < 1.33$. It should be noticed that a recirculating flow must occur in this region, because of the location of the injectors. Except for this fact, the structure flow is similar to the previous one for the axial velocity component [Fig. 8(a)]. The X-component of the mean time velocity field was investigated for several sections of the tube: these results have been reported in dimensionless form in Fig. 8(c). Between $X/D \approx 5$ and $X/D = 9$ (exit section), the profiles remain similar with a constant decreasing of the turbulence intensity, as seen from Fig. 8(b). Figure 8(b) also shows that the values of the turbulence intensity are lower than for the axial injector system (due to the definition of dimensionless variables). In our configuration of the LDA procedure, the incident beams are normal to the axis of the tube, so that it was experimentally difficult to perform measurements near the walls because of the reflection of the laser beams. It follows that the recirculating zone which approximately occurs between $0.7 \leqslant r/R < 1$ (for low values of the ratio X/D) does not clearly appear in Fig. 8. It should be noticed that the LDA bench was not equiped with a Bragg cell, so that negative values of the velocity could not be measured. However, extrapolation of the curves show that gas flow-rate conservation is verified.

Compared to the above results, Fig. 9(a) and (b) shows the effect of Re on the axial component velocity [Fig. 9(a)] and the accompanying turbulence intensity [Fig. 9(b)]: we see that the reattachment point is nearer the throat region as Re decreases.

3.2. *Temperature field in the discharge tube*

For the two kinds of injector, the temperature profiles in several sections of the discharge tube have been measured during the discharge by using a thermo-

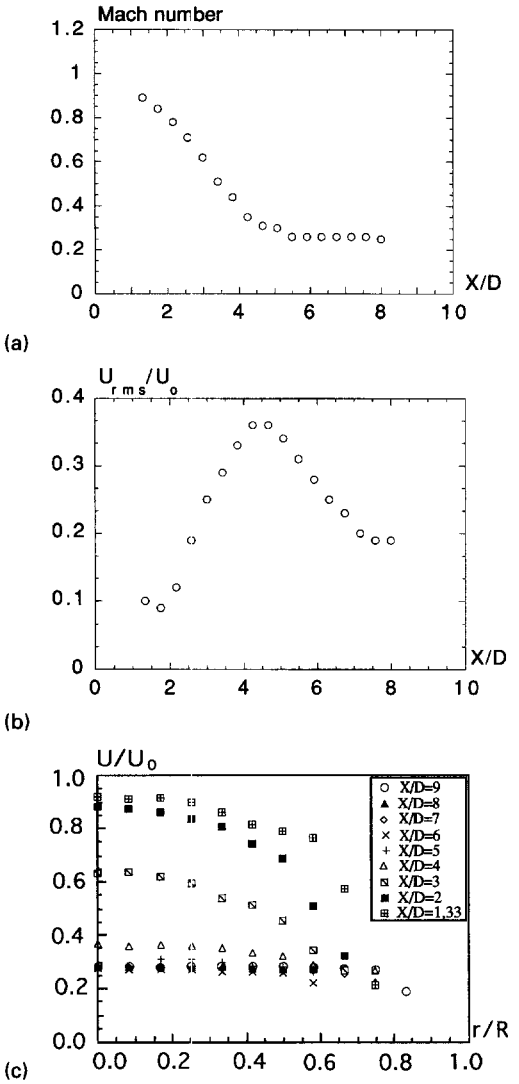

Fig. 8. (a). Variation of the mean time velocity along the axis of the tube (radial injectors). $Re = 17\ 300$, $P_{down} = 50$ mb. (b) Turbulence intensity along the axis of the tube (radial injectors). $Re = 17\ 300$, $P_{down} = 50$ mb. (c) Dimensionless velocity profiles for several sections of the tube. $Re = 17\ 300$, $P_{down} = 50$ mb.

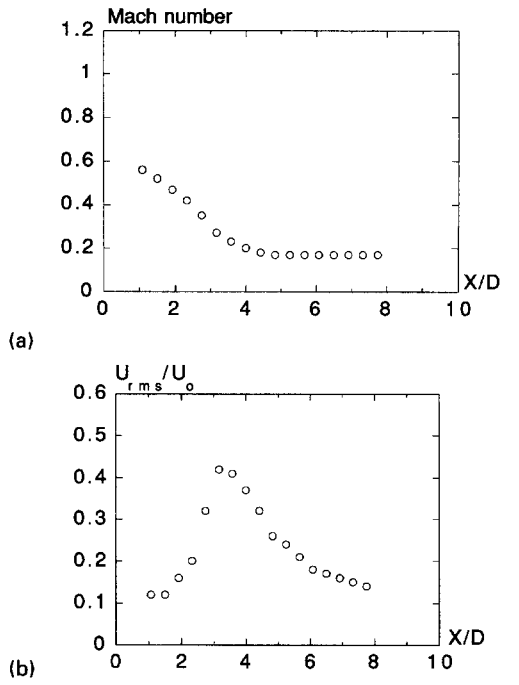

Fig. 9. (a). Variation of the mean time velocity along the axis of the tube (radial injectors). $Re = 12\ 100$, $P_{down} = 50$ mb. (b) Turbulence intensity along the axis of the tube (radial injectors). $Re = 12\ 100$, $P_{down} = 50$ mb.

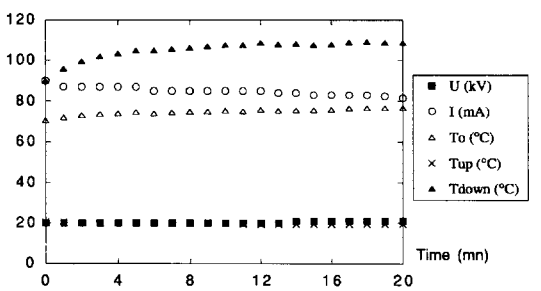

Fig. 10. Variation of the parameters controlling the laser discharge with time. $P_{down} = 41$ mb, $P_v = 1.06$ W cm^{-3}.

fluorescent probe. Several tries and analysis of the electric discharge stability with time have allowed us to determine the experimental values of the intensity and voltage ($I = 50$–100 mA and $V = 20$ kV). The composition of the gas mixture is CO_2 (3%), nitrogen (41%) and helium (56%) The variations of I, V, T_{up} (temperature upstream of the nozzle), T_{down} (temperature downstream of the exit section of the tube) and T_0 (temperature at a point located on the axis) with time are plotted in Fig. 10. We see that the current slowly decreases whereas the voltage increases, so that the energy delivered in the laser mixture is constant during the experiment. It follows that a steady-state regime is reached approximately 15 min after the beginning of the discharge and all the temperatures then remain constant.

3.2.1. *Axial injector.* Temperature as a function of the dimensionless radius r/R has been plotted in Fig. 11(a)–(c), for several sections of the discharge tube and two values of the current intensity (50 and 100 mA), the corresponding power delivered in the discharge being 0.53 and 1.06 W cm^{-3}, respectively. The abscissa $r/R = -1$ corresponds to the wall tube, where the probe is introduced.

The first profile [Fig. 11(a)] shows the temperature distribution in a section located near the nozzle and the minimal temperature is observed on the axis ($r/R = 0$). In the recirculating zone, the temperatures increase because the velocities are smaller for the same

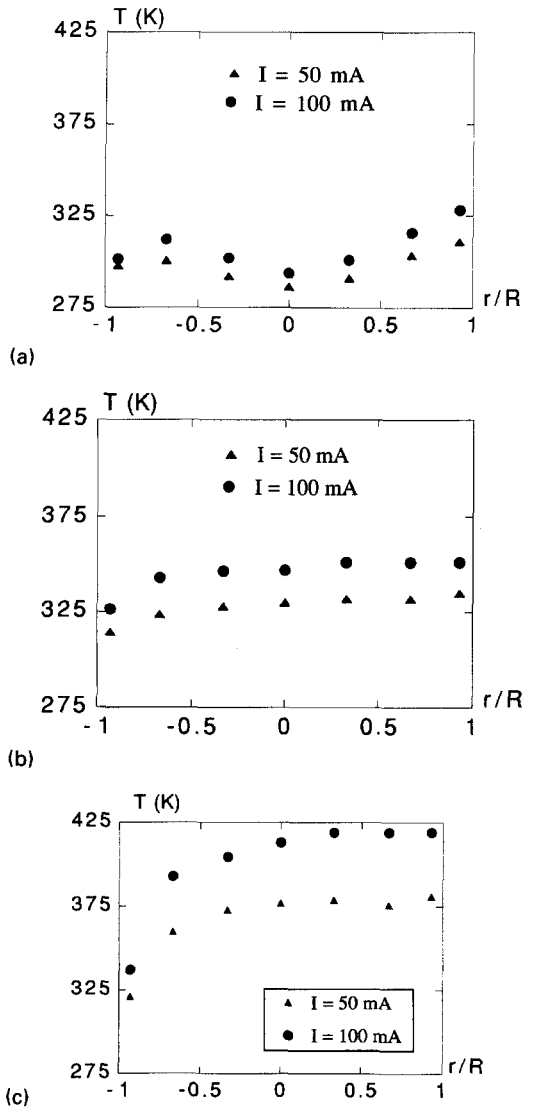

Fig. 11. (a) Temperature profile near the nozzle ($X/D = 1.7$) for the axial injector. $Re = 6700$, $P_{down} = 30$ mb. (b) Temperature profile downstream of the reattachment zone ($X/D = 4.1$) for the axial injector. $Re = 6700$, $P_{down} = 30$ mb. (c) Temperature profile near the exit section ($X/D = 7.9$) for the axial injector. $Re = 6700$, $P_{down} = 30$ mb.

value of the heat source. After the reattachment point $\{X/D = 4.1$ [Fig. 11(b)]$\}$, the radial temperature profile is flattened. The shape of this profile is the same near the exit section $\{X/D = 7.9$ [Fig. 11(c)]$\}$, but the temperature difference between the axis and the wall increases with X/D. This variation is quasi-linear, as shown in Fig. 12.

It should be noticed that the density of the electrical energy delivered is symmetrical about the axis of the tube. This has been verified by studying the stability of the discharge luminosity during the experiments. Figure 13(a) illustrates the discharge luminosity in the

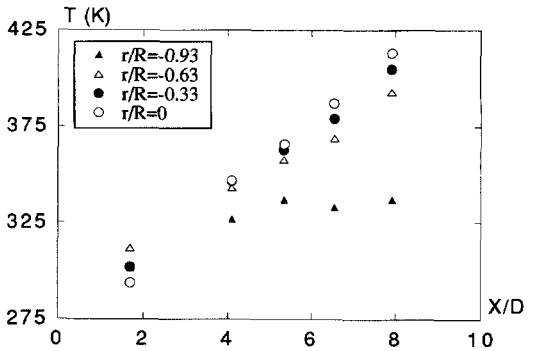

Fig. 12. Variation of temperature along the discharge tube. $Re = 6700$, $P_{down} = 30$ mb.

first half of the tube: this picture was realized by using a CCD camera with an exposure time ranging from 1/20 to 1/500 s. Figure 13(b) shows the corresponding radial distribution of luminosity for several sections of the tube: except for near the throat ($X/D = 0.66$ and 1.32), we see that the symmetry is good and that the turbulence produces a good homogenization of the discharge throughout the tube. Indeed, the turbulence process aids the mixing of the charged particles and these are then uniformly distributed in the whole volume of the tube. However, as seen from Fig. 11(b) and (c), this symmetry does not appear on the temperature profiles. This phenomenon is mainly due to conductive losses in the probe [10], as explained in the Appendix.

3.2.2. *Radial injectors.* As for the previous case, Fig. 14(a)–(c), respectively, shows the radial temperature profiles in sections located near the injection system (a), after the reattachment zone (b) and near the exit of the discharge tube (c). Figure 15 illustrates the axial variation of the temperatures. The shape of the temperature profiles is very similar to the previous case. However, the exit temperature is lower because the mass flow-rate is higher for this injection system (15 g s^{-1}). For $X/D = 2.1$ [Fig. 14(a)], the minimal temperature is again observed on the axis of the discharge tube (where the velocity is higher) and its maximal value is reached in the recirculation zone. Figure 14(b) and (c) shows an increasing temperature between the reattachment point and the exit section, and this variation is quasi-linear as shown in Fig. 15. It is noticed that the radial temperature profile is not symmetrical with respect to the axis of the tube. However, Fig. 16(a) and (b) again shows the symmetry of the laser discharge.

4. CONCLUSION

We have presented an experimental investigation of the velocity and temperature fields in a cylindrical discharge tube. The case of gas injection by means of either a single axial sonic nozzle or 12 sonic nozzles

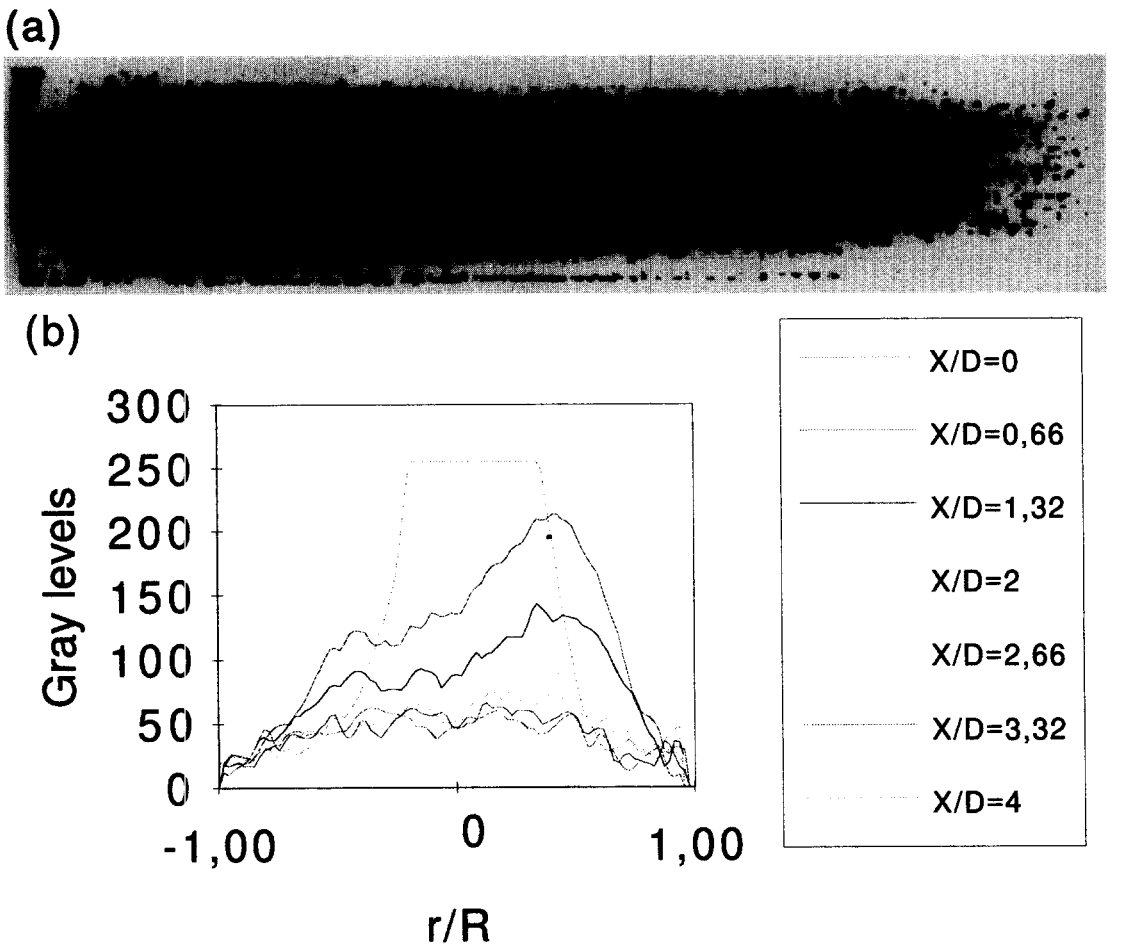

Fig. 13. (a) Visualization of the discharge in the first half part of the discharge tube (axial injector). $Re = 6700$, $P_{down} = 30$ mb. (b) Radial variation of luminosity for several sections (axial injector). $Re = 6700$, $P_{down} = 30$ mb.

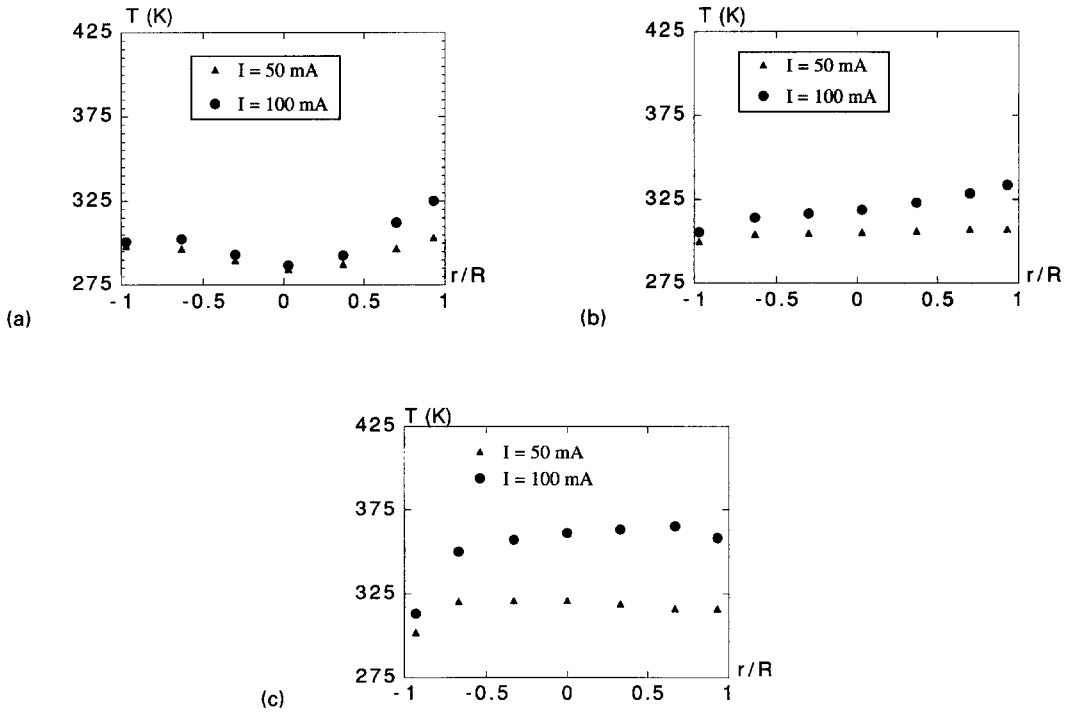

Fig. 14. (a) Temperature profile near the nozzle ($X/D = 2.1$) for the radial injectors. $Re = 17\,300$, $P_{down} = 50$ mb. (b) Temperature profile downstream of the reattachment zone (X/D) = 4.5) for the radial injectors. $Re = 17\,300$, $P_{down} = 50$ mb. (c) Temperature profile near the exit section ($X/D = 8.3$) for the radial injectors. $Re = 17\,300$, $P_{down} = 50$ mb.

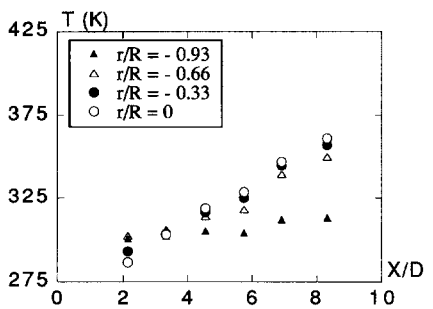

Fig. 15. Variation of temperature along the discharge tube (radial injectors). $Re = 17\,300$, $P_{down} = 50$ mb.

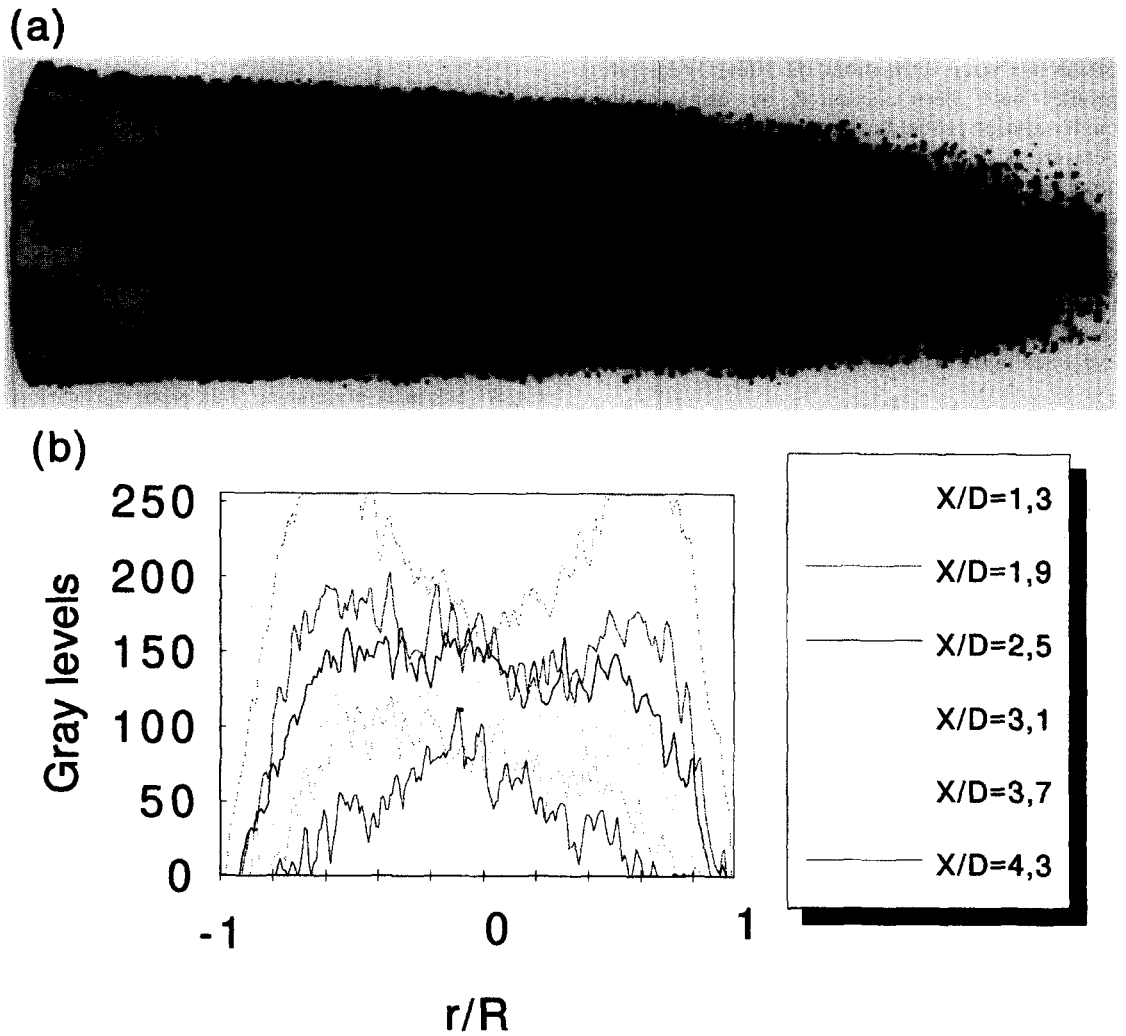

Fig. 16. (a) Visualization of the discharge in the first half part of the discharge tube (radial injectors). $Re = 17\ 300$, $P_{down} = 50$ mb. (b) Radial variation of luminosity for several sections (radial injectors). $Re = 17\ 300$, $P_{down} = 50$ mb.

radially arranged has been examined. The velocity field was measured with the LDA technique. The results show that the flow structure is highly turbulent and similar for the two injection systems, except for near the entrance region of the discharge tube (near the nozzles). It is shown that the turbulence intensity is higher for the axial injector system and that the turbulence allows us to obtain a good homogenization of the discharge throughout the tube. Temperature profiles have been measured by using a thermofluorescent probe during the discharge. The temperature is approximately a linear function of the abscissa X/D. The study of the stability of the discharge luminosity shows the symmetry of the flow structure, which is in agreement with the measured velocity profiles. On the other hand, the symmetry of the temperature profiles is not observed, but this can result from the conductive losses in the probe, as explained in the Appendix.

REFERENCES

1. H. Maillet, *Le laser: principes et techniques d'application.* Tech. et Doc., Paris (1986).
2. J. P. Reilly, CO_2 electric discharge lasers: present status and future applications, Technical note.
3. H. Brunet, M. Mabru and M. Gastaud, Characteristics of turbulent flow stabilized DC-discharges for CO_2 lasers, *Proceedings of the 6th Gas Flow and Chemical Lasers International Symposium*, pp. 40–43. Springer-Verlag, Berlin (1986).
4. Trollat, Etude expérimentale d'un écoulement turbulent de N_2, Report from Ecole Centrale de Paris (1987).
5. H. Brunet and J. Rocca Serra, Model for glow discharge in flowing nitrogen, *J. Appl. Phys.* **57,** 1574–1581 (1985).
6. J. D. Miler and J. S. Chang, A numerical model for the positive column of a glow discharge in a gas flow at low and moderate Reynolds numbers, *J. Phys. D: Appl. Phys.* **19,** 565–574 (1986).
7. M. Hégo, Mesures de vitesses dans un tube cylindrique an aval d'une expansion abrupte, Rapport interne, Ecole Centrale de Paris (1988).
8. P. Kolodner, A. Katzir and N. Hartsough, Noncontact surface temperature measurement during reactive-ion etching using fluorescent polymer films, *Appl. Phys. Lett.* **42,** 749–751 (1983).
9. P. Kolodner and J. A. Tyson, Remote thermal imaging with 0.7 μm spatial resolution using temperature dependent fluorescent thin films, *Appl. Phys. Lett.* **42,** 117–119 (1983).
10. O. Boiron, Caractérisation aérothermique d'un laser CO_2 de puissance à flux axial rapide, Thesis, University Aix-Marseille II, France (1992).
11. W M. Roshenow and J. P. Harnett, *Handbook of Heat Transfer.* McGraw-Hill, New York (1985).

APPENDIX: THERMAL ANALYSIS OF THE PROBE

As pointed out above (Section 3.2), the conductive heat transfer through the probe can greatly affect the measured temperature, specially when the temperature sensor is located in a flow subjected to high temperature gradients, which is the case near the walls of the discharge tube.

Figure A1 schematically presents the cylindrical probe, y being the axis of this cylinder. It consists of several materials: alumina, glass, quartz, fluorogermanate and ceramic. The width of the fluorogermanate layer ranges from 10 to 20 μm

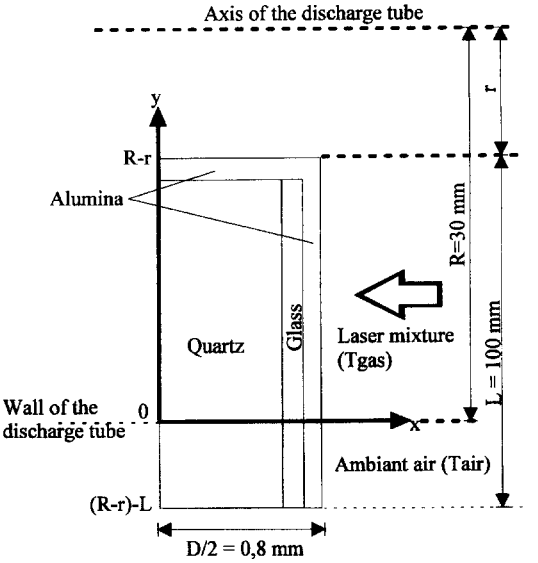

Fig. A1. Schematic presentation of the probe and definition of coordinates.

so that its physical properties can be assumed equal to the quartz without introducing a significant error. For the same reason, the ceramic top of the probe is assumed to be made with alumina (the mass of alumina in the chemical composition of ceramics generally ranges from 90 to 99.8%). As seen from Fig. A1, the probe is subjected to several heat fluxes:

(i) the forced convection between the gas mixture and the top and lateral surface of the probe;

(ii) the radiative exchange between the probe and the wall of the discharge tube: it can easely be shown that this flux is negligible, as is the radiative exchange between the probe and the ambient air (for $0 < y < R-r-L$);

(iii) the conduction in the probe;

(iv) the convective exchange between the probe and ambient air (for $0 < y < R-r-L$)

With the above assumptions, the temperature distribution in the probe, $T(x, y, t)$, is obtained by solving the following differential system of equations:

$$\rho_i Cp_i \frac{\partial T}{\partial t} = \mathrm{Div}\,(k_i \vec{\mathrm{grad}}\, T) \tag{A1}$$

where i refers to one of the three materials, which means that there are three equations; ρ, Cp and k, respectively, denote the density, specific heat and thermal conductivity of material i. The continuity of flux is written for all the interfaces by applying Fourier's law and neglecting the contact thermal resistances. Because of symmetry, the others boundary conditions are:

$$\frac{\partial T(0, y, t)}{\partial x} = 0 \tag{A2}$$

$$k_{\mathrm{Al}} \frac{\partial T(0, R-r, t)}{\partial y} = h_{\mathrm{p}} S_{\mathrm{p}} (T_{\mathrm{gas}} - T_{\mathrm{probe}}) \quad \text{for} \quad 0 < x < D/2 \tag{A3}$$

$$k_{\mathrm{Al}} \frac{\partial T(0, R-r-L, t)}{\partial y} = 0 \quad \text{for} \quad 0 < x < D/2 \tag{A4}$$

$$k_{\mathrm{Al}} \frac{\partial T(D/2, y, t)}{\partial x} = h_{\mathrm{C}} S_{\mathrm{C}} (T_{\mathrm{gas}} - T_{\mathrm{probe}}) \quad \text{for} \quad 0 < y < R-r \tag{A5}$$

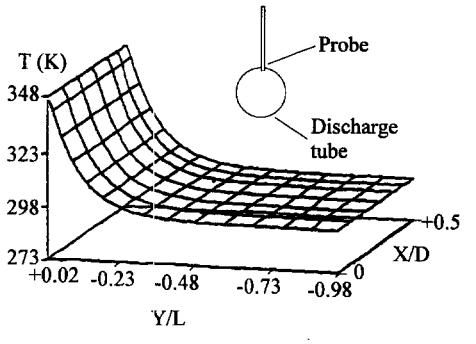

(a)

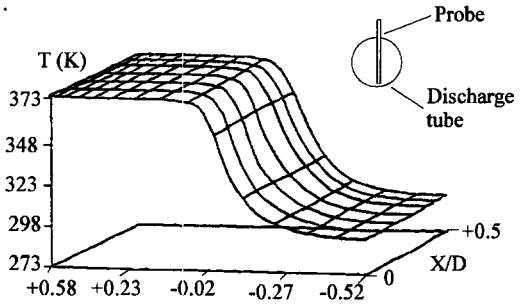

(b)

Fig. A2. (a) Temperature distribution in the probe when its lateral surface is subjected to a uniform temperature distribution: the temperature sensor is located at $r = -2$ mm. (b) Temperature distribution in the probe when its lateral surface is subjected to a uniform temperature distribution: the temperature sensor is located at $r = +58$ mm.

$$k_{Al}\frac{\partial T(D/2, y, t)}{\partial x} = h_{CN}S(T_{air} - T_{probe})$$

for $0 < y < R - r - L$. (A6)

In the above equations, the subscript 'Al' refers to alumina, whereas h_p is the convective heat transfer coefficient between the surface at the top (S_p) and the laser mixture; h_c is the convective heat transfer coefficient between the lateral surface of the probe (S_C) and the laser mixture; h_{CN} is the convective heat transfer coefficient between the external lateral surface of the probe (S) and the ambient air. The differential system of equation (A1) subjected to boundary conditions (A2)–(A6) was solved by using the MEF/MOSAIC code, which uses a finite-element procedure.

Figure A2(a) and (b) shows the temperature distribution

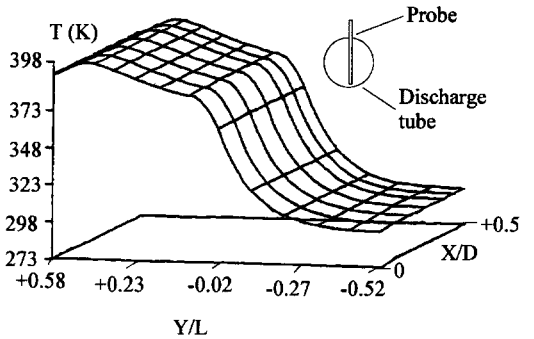

Fig. A3. Temperatures in the probe when its lateral surface is subjected to a non-uniform temperature distribution: the temperature sensor is located at $r = +58$ mm.

as a function of the position of the probe in the discharge tube. For these calculations, the initial value of the probe temperature was 293 K and the temperature of the gas was 373 K. The values of the heat transfer coefficients have been calculated by using the classical correlations for Nusselt numbers [11] and the value of the mean velocity was deduced from the measurements. The ratio between the length and the radius of the probe, $L/(D/2)$, is equal to 125. In the case of Fig. A2(a), the top of the probe is located at $y = 2$ mm from the inner wall of the tube (that is at $r = 28$ mm from the axis of the tube). We see that the temperature of the top, which is the measured temperature, is smaller (75°C) than the real fluid temperature (100°C): this difference results from the conductive losses through the cylinder, most of its lateral surface being cooled by ambient air. Because the surface in contact with the hot gas is higher as the probe is introduced in the discharge tube, such a difference is not observed when the temperature sensor is located on the axis or near the opposite wall [Fig. 18(b), $y = 58$ mm]. However, for this last case, another thermal phenomenon occurs because the sensor is in the thermal boundary layer, and so the lateral surface of the cylinder is again subjected to high velocity and temperature gradients. This case has been modeled in Fig. A3 by assuming a variable temperature distribution on the lateral surface: for these calculations the temperature of the gas has a symmetrical linear variation between 100°C (wall) and 120°C (axis of the discharge tube). For this example, the difference between the measured and the real temperature is then equal to 10°C.

The above analysis shows that a measured non-symmetrical temperature profile can result from the conduction process in the probe, even if the real temperature profile is symmetrical. Such a situation occurs when the probe is subjected to high temperature gradients, which is the case when the temperature sensor is located near the walls.